

Partonic Transverse Motion in Unpolarized Semi-Inclusive Deep Inelastic Scattering

M. Boggione^{*}, S. Melis[†] and A. Prokudin^{**}

^{*}*Dipartimento di Fisica Teorica, Università di Torino, Via P. Giuria 1, I-10125 Torino, Italy
INFN, Sezione di Torino, Via P. Giuria 1, I-10125 Torino, Italy*

[†]*European Centre for Theoretical Studies in Nuclear Physics and Related Areas (ECT^{*})
Villa Tambosi, Strada delle Tabarelle 286, I-38123 Villazzano, Trento, Italy*

^{**}*Jefferson Laboratory, 12000 Jefferson Avenue, Newport News, VA 23606*

Abstract. We analyse the role of partonic transverse motion in unpolarized Semi-Inclusive Deep Inelastic Scattering (SIDIS) processes. Imposing appropriate kinematical conditions, we find some constraints which fix an upper limit to the range of allowed k_{\perp} values and lead to interesting results, particularly for some observables like the $\langle \cos \phi_h \rangle$ azimuthal modulation of the unpolarized SIDIS cross section and the average transverse momentum of the final, detected hadron.

Keywords: SIDIS, parton intrinsic transverse momentum, azimuthal moments

PACS: 13.88.+e, 13.60.-r, 13.85.Ni

Azimuthal spin asymmetries in SIDIS processes are directly related to Transverse Momentum Dependent (TMD) parton distribution and fragmentation functions, and are the subject of intense theoretical and experimental studies. The usual, collinear parton distribution functions depend on the fraction x_b of hadron momentum carried by the scattering parton and on the virtuality of the probe, Q^2 . Additionally, TMDs depend on the intrinsic transverse momentum of the parton, \mathbf{k}_{\perp} , opening invaluable opportunities to unravel the three-dimensional partonic picture of the nucleon in momentum space.

In phenomenological analysis, the transverse momentum distribution of the TMDs is usually assumed to be a Gaussian. This is a convenient approximation as it allows to solve the k_{\perp} integration analytically, and it leads to a successful description of many sets of data. Inspired by the parton model, we bound the integration range of transverse momenta k_{\perp} and we observe, in some kinematical regions, remarkable deviations from the predictions obtained from the common TMD approach, based on the Gaussian parametrization integrated over the full k_{\perp} range, $[0, \infty]$. We show that some kinematical ranges, typically low x_b or equivalently low Q^2 regions, are not safely controlled by the present phenomenological model, while a physical upper limit on the k_{\perp} range can prevent uncontrolled large k_{\perp}/Q contributions. This leads, for instance, to a better description of some observables like the $\langle \cos \phi_h \rangle$ asymmetry and introduces some interesting effects in the $\langle P_T^2 \rangle$ behaviors.

We study the SIDIS process in the γ^* - proton c.m. frame, where γ^* denotes the virtual photon. The detailed kinematics is given in Refs. [1, 2, 3].

A physical picture that allows us to put some further constraints on the partonic intrinsic motion is provided by the parton model, where kinematical limits on the transverse momentum size can be obtained by requiring the energy of the parton to be

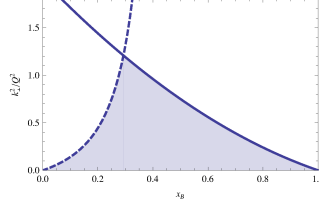


FIGURE 1. k_{\perp}^2/Q^2 phase space as determined by the bounds of Eqs. (1) and (2). The allowed region, which fulfills both bounds, is represented by the shaded area below the solid line.

less than the energy of the parent hadron and by preventing the parton to move backward with respect to the parent hadron direction ($k_z < 0$). They give, respectively:

$$k_{\perp}^2 \leq (2 - x_B)(1 - x_B)Q^2, \quad 0 < x_B < 1. \quad (1)$$

and

$$k_{\perp}^2 \leq \frac{x_B(1 - x_B)}{(1 - 2x_B)^2}Q^2, \quad x_B < 0.5. \quad (2)$$

Notice that these are exact relations, which hold at all orders in (k_{\perp}/Q) .

The ratio k_{\perp}^2/Q^2 , as constrained by Eqs. (1) and (2), is shown in Fig. 1 as a function of x_B : from this plot it is immediately evident that although in principle Eq. (2) (represented by the dashed line) gives a stringent limit on k_{\perp}^2/Q^2 in the region $x_B < 0.5$, it intercepts the bound of Eq. (1) (solid line) in $x_B \simeq 0.3$, where the latter becomes most relevant. Notice also that present data from HERMES and COMPASS experiments span the region $x_B \leq 0.3$, where only the momentum bound of Eq. (2) plays a role.

Once the maximum value of k_{\perp} is limited by Eqs. (1) and (2), we set the appropriate normalization coefficient

$$f_{q/p}(x, k_{\perp}) = f_{q/p}(x) \frac{1}{1 - e^{-(k_{\perp}^{\max})^2/\langle k_{\perp}^2 \rangle}} \frac{e^{-k_{\perp}^2/\langle k_{\perp}^2 \rangle}}{\pi \langle k_{\perp}^2 \rangle}, \quad (3)$$

where $(k_{\perp}^{\max})^2$ denotes the maximum value of k_{\perp}^2 for each given values of x_B and Q^2 as required by Eqs. (1), and (2), so that

$$f_{q/p}(x) = \int_0^{2\pi} d\phi \int_0^{k_{\perp}^{\max}} k_{\perp} dk_{\perp} f_{q/p}(x, k_{\perp}). \quad (4)$$

The average hadronic transverse momentum $\langle P_T^2 \rangle$ of the final, detected hadron h is defined as:

$$\langle P_T^2 \rangle = \frac{\int d^2\mathbf{P}_T P_T^2 d\sigma}{\int d^2\mathbf{P}_T d\sigma}. \quad (5)$$

Notice that if the integral is performed over the range $[0, \infty]$, then $\langle P_T^2 \rangle$ coincides with the Gaussian width of the unpolarized P_T distribution of the SIDIS cross section: $\langle P_T^2 \rangle \equiv \langle P_T^2 \rangle_G \equiv \langle p_{\perp}^2 \rangle + z_h^2 \langle k_{\perp}^2 \rangle$. The experimental P_T range, however, usually span a finite region between some P_T^{\min} and P_T^{\max} ; therefore, in any experimental analysis, one inevitably has

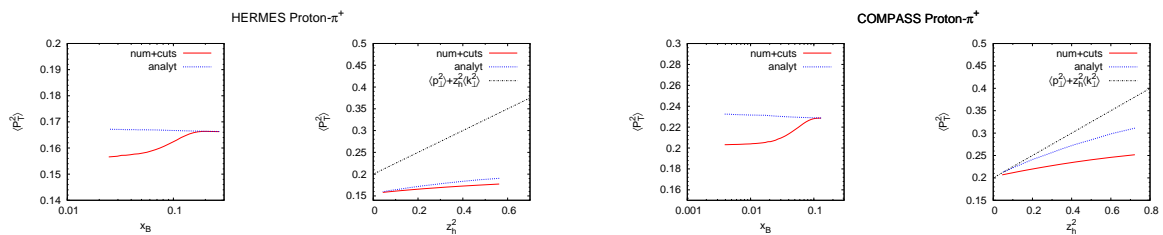


FIGURE 2. $\langle P_T^2 \rangle$ as a function of x_B (left plot) and of z_h^2 (right plot), for π^+ production at HERMES (right panel) and COMPASS (left panel). The solid (red) line corresponds to $\langle P_T^2 \rangle$ calculated with a numerical integration implementing Eqs. (1) and (2), while the dashed (blue) line is $\langle P_T^2 \rangle$ calculated with an analytical integration. In both cases we have applied the corresponding experimental cuts. The dash-dotted (black) line corresponds to the Gaussian $\langle P_T^2 \rangle_G$.

$\langle P_T^2 \rangle \neq \langle P_T^2 \rangle_G$, even without considering the cuts in Eqs. (1) and (2). Consequently, the relation $\langle P_T^2 \rangle \simeq \langle p_\perp^2 \rangle + z_h^2 \langle k_\perp^2 \rangle$ holds only approximatively.

Figure 2 shows the average hadronic transverse momentum $\langle P_T^2 \rangle$ as a function of x_B and of z_h^2 for π^+ production at HERMES and COMPASS, respectively. The solid (red) lines correspond to $\langle P_T^2 \rangle$ obtained with a numerical k_\perp integrations implementing Eqs. (1) and (2). Instead, the dashed (blue) lines correspond to $\langle P_T^2 \rangle$ computed with an analytical integration. In both cases we have taken into account the appropriate experimental P_T cuts. Clearly, at low x_B , there is a substantial deviation from the analytical calculation, which also affects the value of $\langle P_T^2 \rangle$ as a function of z_h^2 . As far as the z_h dependence is concerned, first of all, one can see that there is a large deviation from the naive formula $\langle P_T^2 \rangle = \langle p_\perp^2 \rangle + z_h \langle k_\perp^2 \rangle$, corresponding to the dash-dotted (black) lines, for both calculations. Secondly, although the z_h^2 -dependence is not linear any more, it seems to be approaching an almost constant behavior

The $\langle \cos \phi_h \rangle$ modulation receives two contributions, both suppressed by one power of (k_\perp/Q) . The Cahn term, which is proportional to the convolution of the unpolarized distribution and fragmentation functions, was extensively studied in Ref. [4]. There, EMC measurements [5] on the $\cos \phi_h$ modulation and of the P_T distribution on the unpolarized SIDIS cross section were used to determine the Gaussian width of the k_\perp distribution of the unpolarized distribution function $f_{q/p}(x, k_\perp)$. The second term is proportional to the convolution of the Boer-Mulders distribution function and the Collins fragmentation function and was neglected in Ref. [4].

Figures 3 and 4 show how a large deviation from the analytical integration results is obtained by applying the k_\perp bounds of Eqs. (1) and (2) when computing the Cahn effect contribution to $\langle \cos \phi_h \rangle$ corresponding to the HERMES and COMPASS kinematics. In these figures our results, obtained with and without k_\perp - cuts, are compared to the latest HERMES [6] and COMPASS [7] data. Although still showing a considerable deviation from the experimental data, our calculation confirms that physical partonic cuts have a quite dramatic effect in the small x region, and should therefore be taken into account in any further analysis of these experimental data.

To evaluate the influence of the partonic cuts on the contribution to $\langle \cos \phi_h \rangle$ originating from the Boer-Mulders \otimes Collins term, we use the parametrization of Ref. [8] for the

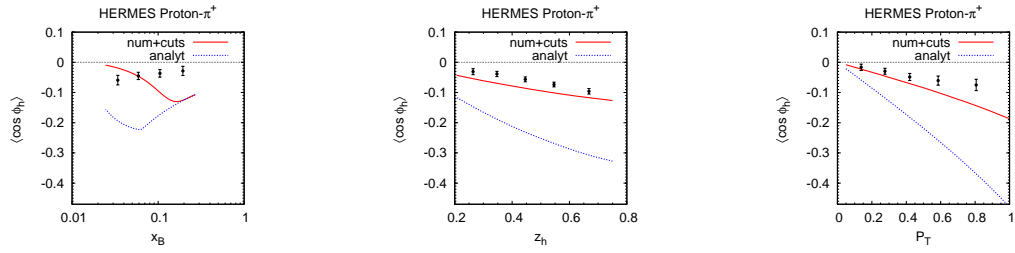


FIGURE 3. Cahn contribution to $\langle \cos \phi_h \rangle$ for π^+ production at HERMES, as a function of x_B (left plot), z_h (central plot) and P_T (right plot). The solid (red) line corresponds to $\langle \cos \phi_h \rangle$ calculated with a numerical k_\perp integration over the range $[0, k_\perp^{max}]$. The dashed (blue) line is $\langle \cos \phi_h \rangle$ obtained by integrating over k_\perp analytically. The full circles are preliminary experimental data from Ref. [6].

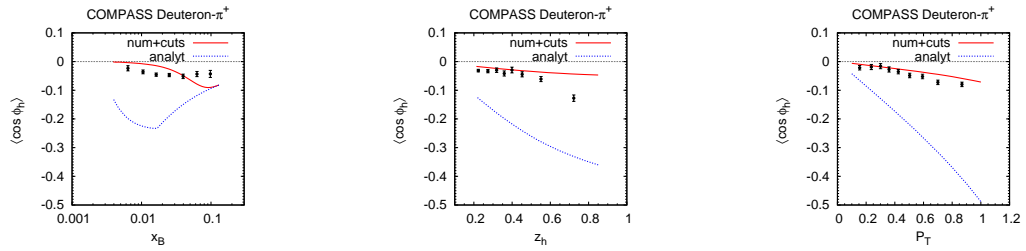


FIGURE 4. Same as Fig. 3, for the COMPASS kinematics. The full circles are preliminary experimental data from Ref. [7].

Collins function while for the Boer-Mulders function we apply the extraction of Ref [9]. The Boer-Mulders contribution is very tiny and is not strongly affected by kinematical cuts of Eqs. (1) and (2).

The residual discrepancy between the model prediction and the measurements of the $\langle \cos \phi_h \rangle$ azimuthal moment could indicate that higher twist contributions, from pure twist-3 functions, for example, might be non negligible in this modulation. More elaborated phenomenological studies including twist-3 TMDs would be necessary to confirm these observation.

REFERENCES

1. M. Anselmino, et al., *Phys. Rev.* **D73**, 014020 (2006), hep-ph/0509035.
2. M. Anselmino, M. Boglione, U. D'Alesio, S. Melis, F. Murgia, E. Nocera, and A. Prokudin, *Phys. Rev.* **D83**, 114019 (2011), 1101.1011.
3. M. Boglione, S. Melis, and A. Prokudin (2011), 1106.6177.
4. M. Anselmino, M. Boglione, U. D'Alesio, A. Kotzinian, F. Murgia, and A. Prokudin, *Phys. Rev.* **D71**, 074006 (2005), hep-ph/0501196.
5. J. Ashman, et al., *Z. Phys.* **C52**, 361–388 (1991).
6. F. Giordano, and R. Lamb, *PoS DIS2010*, 106 (2010).
7. G. Sbrizzai (2009), 0902.0578.
8. M. Anselmino, et al., *Nucl. Phys. Proc. Suppl.* **191**, 98 (2009), 0812.4366.
9. V. Barone, S. Melis, and A. Prokudin, *Phys. Rev.* **D81**, 114026 (2010), 0912.5194.